Coupled Ferric Oxides and Sulfates on the Martian Surface

J.-P. Bibring, *et al.*

Science **317**, 1206 (2007);
DOI: 10.1126/science.1144174

Science (print ISSN 0036-8075; online ISSN 1095-9203) is published weekly, except the last week in December, by the American Association for the Advancement of Science, 1200 New York Avenue NW, Washington, DC 20005.

mational changes at the periphery of the molecule, and is well-suited for use in self-assembled monolayers. Another advantage is that the symmetry inherent to the system implies that both positions of the switch have the same total energy and do not differ in binding to the substrate. Thus, we could observe this switching process, on a variety of insulating films (NaCl, RbI, and Xe), for two related molecules (phthalocyanine and naphthalocyanine) and for different charge states of the molecules. These measurements demonstrate the robustness of the process, and given that no changes occur in the molecular framework, it can be anticipated that the switching will also work with molecules embedded in all solid-state devices and in multicore porphyrin-class molecules acting as more complex devices.

References and Notes

1. D. M. Eigler, C. P. Lutz, W. E. Rudge, *Nature* **352**, 600 (1991).
2. C. Joachim, J. K. Gimzewski, A. Aviram, *Nature* **408**, 541 (2000).
3. A. Nitzan, M. A. Ratner, *Science* **300**, 1384 (2003).
4. Y. Selzer, D. L. Allara, *Annu. Rev. Phys. Chem.* **57**, 593 (2006).
5. N. J. Tao, *Nat. Nanotech.* **1**, 173 (2006).
6. C. P. Collier *et al.*, *Science* **289**, 1172 (2000).
7. F. Moresco *et al.*, *Phys. Rev. Lett.* **86**, 672 (2001).
8. X. H. Qiu, G. V. Nazin, W. Ho, *Phys. Rev. Lett.* **93**, 196806 (2004).
9. V. Iancu, S.-W. Hla, *Proc. Natl. Acad. Sci. U.S.A.* **103**, 13718 (2006).
10. Experiments were carried out on a Cu(111) surface with NaCl and Xe insulating layers, on Cu(100) and Cu(311) with NaCl, on Cu(331) with RbI, and on bare Cu(100). Cu single crystals were cleaned by several sputtering-annealing cycles, and thermal evaporation was used to deposit NaCl or RbI so that defect-free, (100)-terminated islands of up to three atomic layers were formed.
11. R. Bennewitz *et al.*, *Surf. Sci.* **438**, 289 (1999).
12. J. Repp, G. Meyer, S. M. Stojkovic, A. Gourdon, C. Joachim, *Phys. Rev. Lett.* **94**, 026803 (2005).
13. J. Repp, G. Meyer, S. Paavilainen, F. E. Olsson, M. Persson, *Phys. Rev. Lett.* **95**, 225503 (2005).
14. A. A. Granovsky, PC GAMESS version 7.0, http://classic.chem.msu.su/gran/gamess/index.html.
15. D. K. Maity, T. N. Truong, *J. Porphyrins Phthalocyanines* **5**, 289 (2001).
16. J. Repp, G. Meyer, F. E. Olsson, M. Persson, *Science* **305**, 493 (2004).
17. B. C. Stipe *et al.*, *Phys. Rev. Lett.* **78**, 4410 (1997).
18. H. J. Lee, W. Ho, *Science* **286**, 1719 (1999).
19. S.-W. Hla, L. Bartels, G. Meyer, K.-H. Rieder, *Phys. Rev. Lett.* **85**, 2777 (2000).
20. J. R. Hahn, W. Ho, *Phys. Rev. Lett.* **87**, 166102 (2001).
21. M. Lastapis *et al.*, *Science* **308**, 1000 (2005).
22. X. H. Qiu, G. V. Nazin, W. Ho, *Phys. Rev. Lett.* **92**, 206102 (2004).
23. D. M. Eigler, E. K. Schweizer, *Nature* **344**, 524 (1990).
24. Phthalocyanine molecules on a monolayer of RbI are negatively charged. The LUMO becomes a singly occupied molecular orbital that can be probed at either negative or positive bias, corresponding to electron removal or addition, respectively (*25*).
25. J. Repp, G. Meyer, S. Paavilainen, F. E. Olsson, M. Persson, *Science* **312**, 1196 (2006).
26. A. Szuchmacher Blum *et al.*, *Nat. Mater.* **4**, 167 (2005).

27. We thank R. Allenspach and M. Grifoni for fruitful discussions. We acknowledge partial funding by European Union projects "CHIC," "NANOMAN," and "NAPA," and by the Volkswagen foundation and the Swiss National Centre of Competence in Research through their "Lichtenberg" and "Nanoscale Science" programs, respectively.

Supporting Online Material

www.sciencemag.org/cgi/content/full/317/5842/1203/DC1
Fig. S1

27 April 2007; accepted 17 July 2007
10.1126/science.1144366

Coupled Ferric Oxides and Sulfates on the Martian Surface

J.-P. Bibring,[1]* R. E. Arvidson,[2] A. Gendrin,[1] B. Gondet,[1] Y. Langevin,[1] S. Le Mouelic,[3] N. Mangold,[4] R. V. Morris,[5] J. F. Mustard,[6] F. Poulet,[1] C. Quantin,[4] C. Sotin[3]

The Mars Exploration Rover (MER), Opportunity, showed that layered sulfate deposits in Meridiani Planum formed during a period of rising acidic ground water. Crystalline hematite spherules formed in the deposits as a consequence of aqueous alteration and were concentrated on the surface as a lag deposit as wind eroded the softer sulfate rocks. On the basis of Mars Express Observatoire pour la Minéralogie, l'Eau, les Glaces et l'Activité (OMEGA) orbital data, we demonstrate that crystalline hematite deposits are associated with layered sulfates in other areas on Mars, implying that Meridiani-like ground water systems were indeed widespread and representative of an extensive acid sulfate aqueous system.

In association with sulfate deposits discovered and mapped inside Valles Marineris, Terra Meridiani, and Margaritifer Terra, ferric oxides have been identified with OMEGA/Mars Express through distinct spectral signatures. These oxides occur in close association with sulfate-rich layered deposits and in low-albedo sand at the base of the deposits. The ferric oxides may thus have formed contemporaneously with sulfate deposits or subsequently (e.g., by diagenetic processes). In either case, the spectral and spatial similarities imply that the formation pathways for sulfate and ferric oxide could have been the same in Valles Marineris and Terra Meridiani, and they likely mimic the geological settings seen on the ground by the MER Opportunity in Meridiani Planum (*1*).

OMEGA, the imaging spectrometer onboard the Mars Express orbiter, acquires spectra in the visible and near infrared wavelength range (0.35 to 5.1 μm) with the use of three different detectors (0.35 to 1.0 μm, 0.95 to 2.6 μm, and 2.5 to 5.1 μm). Its spectral sampling ranges from 7 to 20 nm, and its spatial sampling varies from 300 m to 4 km, depending on the position of the spacecraft on its elliptical orbit (*2*). The instrument has now mapped ~90% of the martian surface at the 1.5- to 5-km scale (*3*).

OMEGA spectra from localized regions in Valles Marineris, Terra Meridiani, and Margaritifer Terra are characterized by an absorption edge between 0.4 and ~0.75 μm; a shallow absorption band, visible as a shoulder, between ~0.6 and ~0.75 μm; a reflectivity maximum at ~0.75 μm; an absorption band centered at ~0.9 μm; and a raise in reflectance up to ~1.3 μm (Fig. 1A). These spectral features are diagnostic for the presence of ferric oxides (Fig. 1B) (*4*), where the two absorption bands and absorption edge result from the single-electron transitions of ferric iron (*5*, *6*). Notably, particle size plays an important role in the strength of ferric absorptions. For example, hematite particles with diameters less than ~10 nm do not have a detectable band minimum at ~0.86 μm, whereas particles with a larger diameter have a distinct, very deep band minimum (*6*, *7*). For specular hematite particles, the band minimum is shallow (*8*). In OMEGA spectra of these areas, the depth of the 0.9-μm ferric signatures reaches 50%, which is more than five times as deep as the common ferric signatures associated with martian bright regions (represented in Fig. 1A for comparison). Some spectra show ferric signatures with sulfate hydration features at ~1.9 and ~2.4 μm or ~2.1 and ~2.4 μm.

The spectral features attributed to ferric oxides in the OMEGA spectra are common to many ferric oxides, including hematite (α-Fe_2O_3), goethite [α-$Fe^{3+}O(OH)$], akaganeite [$Fe^{3+}O(OH,Cl)$], schwertmannite [~$Fe_8O_8(OH)_6SO_4 \cdot nH_2O$], lepidocrocite [$\gamma$-FeO(OH)], and ferrihydrite [$Fe^{3+}{}_2O_3 \cdot 5/9(H_2O)$] (*4*). The shape of the ferric feature is distorted when mixed with dust or a minor contribution of olivine or pyroxene. Moreover, oxide signatures can change with temperature, although the spectral changes have been documented only for well-crystalline hematite and goethite (*9*, *10*). Spectral signatures can also strongly depend on oxide crystallinity (*4*). Finally, the ~0.9-μm ferric band is located near a detector change in the OMEGA instrument (~1 μm): The signal-to-noise ratio is lower in this wavelength range, and differences in reflectance between the detectors are commonly observed at

[1]Institut d'Astrophysique Spatiale, Batiment 121, 91405 Orsay Campus, France. [2]Department of Earth and Planetary Sciences, Washington University, St. Louis, MO 63130, USA. [3]Université de Nantes, 2 rue Houssinière, Boîte Postale 92208, 44322 Nantes Cedex 03, France. [4]Interactions et Dynamique des Environnement de Surface, Batiment 509, 91405 Orsay Campus, France. [5]NASA Johnson Space Center, 2101 NASA Parkway, Houston, TX 77058, USA. [6]Geological Sciences, Brown University, Providence, RI 02912, USA.

*To whom correspondence should be addressed. E-mail: bibring@ias.fr

1 μm. Thus, we cannot at present exclude the presence of any of the ferric oxides listed above on the basis of spectral data.

We also considered the presence of ferric sulfate-bearing phases (schwertmannite is one of these). The hydroxysulfate jarosite [(K, Na, H_3O)$Fe_3(SO_4)_2(OH)_6$] was identified in situ by the MER Mossbauer experiment (*11*, *12*). In the near-infrared wavelength range, jarosite is characterized by narrow diagnostic absorptions at ~1.47, ~1.85, and 2.27 μm [i.e., it is a double feature (doublet)], which are not currently detected in OMEGA spectra. Ferric sulfates generally have a symmetric ~0.9-μm absorption band, with a strong decrease in reflectance between 0.7 and

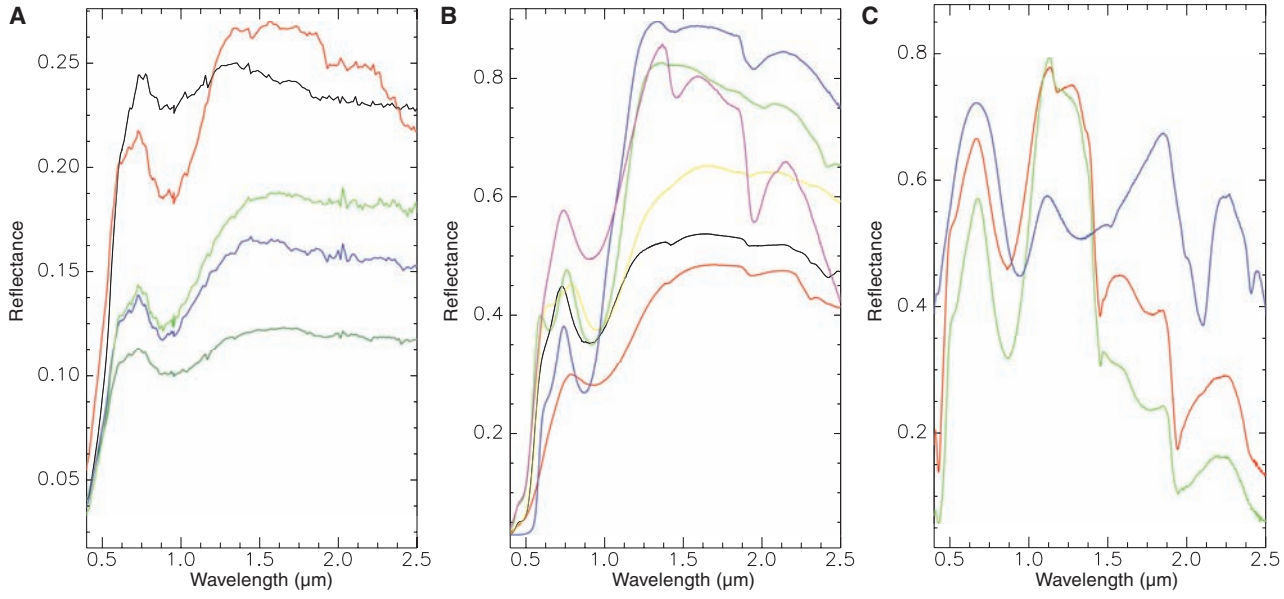

Fig. 1. (**A**) OMEGA spectra of oxide-rich areas, showing Aram Chaos (red), Candor Chasma (light green), Capri Chasma (blue), Meridiani Planum (dark green), and dust for comparison (black). (**B**) Library spectra of the most probable oxides and hydroxides on Mars (*3*) for comparison, including hematite (α-Fe_2O_3) (blue), goethite [α-$Fe^{3+}O(OH)$] (green), lepidocrocite [γ-FeO(OH)] (yellow), akaganeite [$Fe^{3+}O(OH,Cl)$] (black), ferrihydrite [$Fe^{3+}{}_2O_3 \cdot 5/9(H_2O)$] (red), and schwertmannite [~$Fe_8O_8(OH)_6SO_4.nH_2O$] (magenta). The hematite mineral has a small component of water in it, whereas the hematite formula does not contain water (Fe_2O_3). (**C**) Library spectra [reproduced from (*9*)] of ferric and ferrous sulfates, including szomolnokite [$Fe^{2+}SO_4 \cdot (H_2O)$] (blue), copiapite [$Fe^{2+}Fe^{3+}{}_4(SO_4)_6(OH)_2 \cdot 20(H_2O)$] (red), and ferricopiapite [$Fe^{3+}{}_{2/3}Fe^{3+}{}_4(SO_4)_6(OH)_2 \cdot 20(H_2O)$] (green).

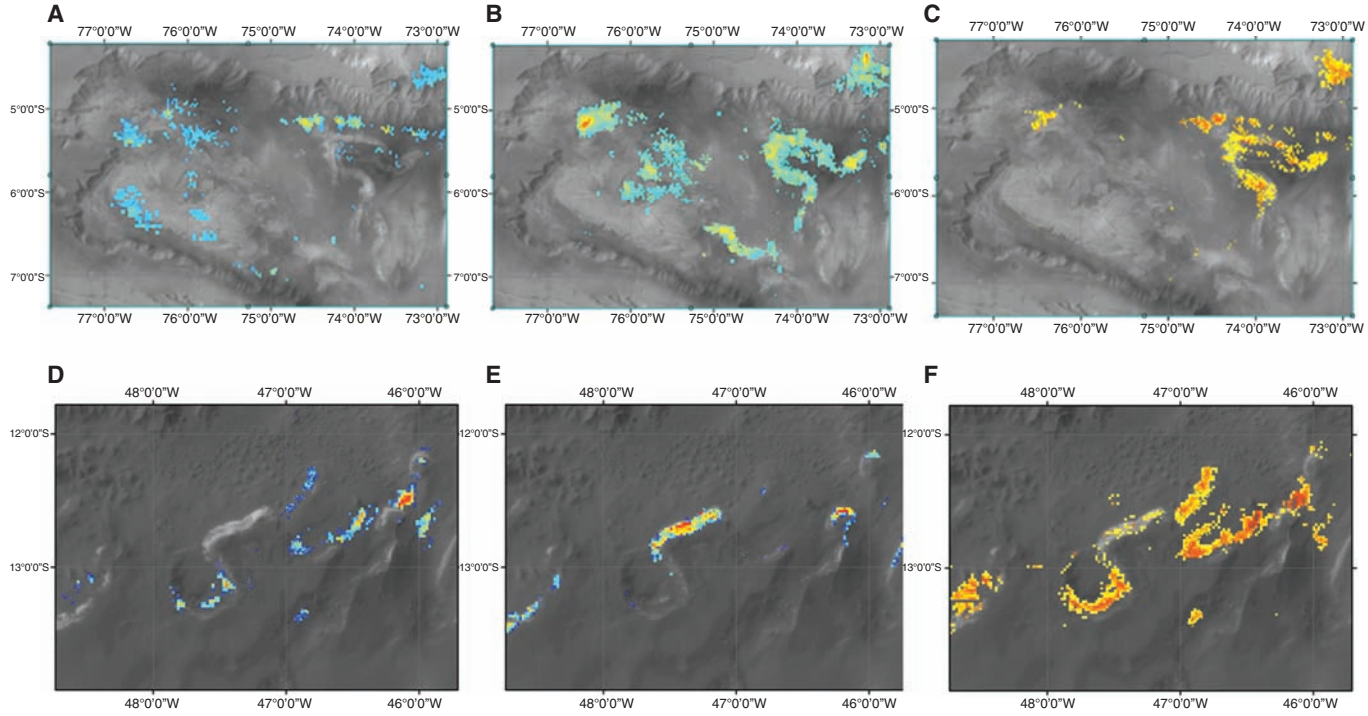

Fig. 2. Spatial association of sulfates and oxides in Candor Chasma [(**A** to **C**), centered at 6°S, 75°W] and Capri Chasma [(**D** to **F**), centered at 13°S, 47°W]. [(A) and (D)] Band depth of 1.9-μm, identified in this case as polyhydrated sulfates (blue = 2%, red ≥ 5%). [(B) and (E)] Band depth of 2.1 μm, identified as kieserite (green = 2%, red ≥ 5%). [(C) and (F)] Oxide band depth, as modeled using the MGM (orange = 10%, red ≥ 30%).

0.9 μm and a strong increase in reflectance between 0.9 and 1.1 μm (*13*), which does not match the very asymmetric OMEGA spectra. Moreover, for similar amplitudes of the 0.9-μm band, the hydration features in the OMEGA spectra—when they are present—are weaker than in ferric sulfate library spectra (Fig. 1C) (*13*). Thus, ferric oxides rather than ferric sulfates constitute the dominant contribution to the spectral signal.

To map the ferric oxides, we used three different methods: the Modified Gaussian Model (MGM) (*14*, *15*), a linear unmixing model (*16*), and the slope between 1.0 and 1.3 μm (using the band ratio between reflectance values at 1.0 and 1.3 μm and selecting the values greater than 15%). The three methods provide concordant results. In Figs. 2 to 4, as well as figs. S1 and S2, we show the results of the MGM-based method. The band depths provided throughout this work represent the strength of the Gaussian corresponding to the ferric component, which is readily distinguished from the pyroxene signatures, as these are coupled to a ~2-μm band. Oxides are identified inside Valles Marineris, Terra Meridiani, and Margaritifer Terra (fig. S1).

In Valles Marineris and Margaritifer Terra, oxides are in close spatial association with the sulfate deposits present in these regions (*17*). Figure 2 shows sulfate and oxide association in Capri and Candor Chasma. However, some sulfate deposits do not have the oxide signature [e.g., kieserite deposits in Capri and Gangis Chasmata and the southernmost gypsum deposit in Iani Chaos (*3*, *17*)]. Oxides are more often associated with polyhydrated sulfates than kieserite (e.g., Capri or Juventae Chasma). Exceptions to this rule are found, for example, on the Candor Mensa deposit, where kieserite and oxides are associated. In Terra Meridiani, oxides are identified both in the hematite-bearing plains and in the etched terrains (*18*). No unambiguous sulfate signature is identified in the hematite-bearing plains (*17*, *19*).

Comparison with the mapping of hematite obtained by the Thermal Emission Spectrometer (TES) onboard the Mars Global Surveyor (MGS) reveals important differences (*20*). In Terra Meridiani, OMEGA identifies oxides throughout

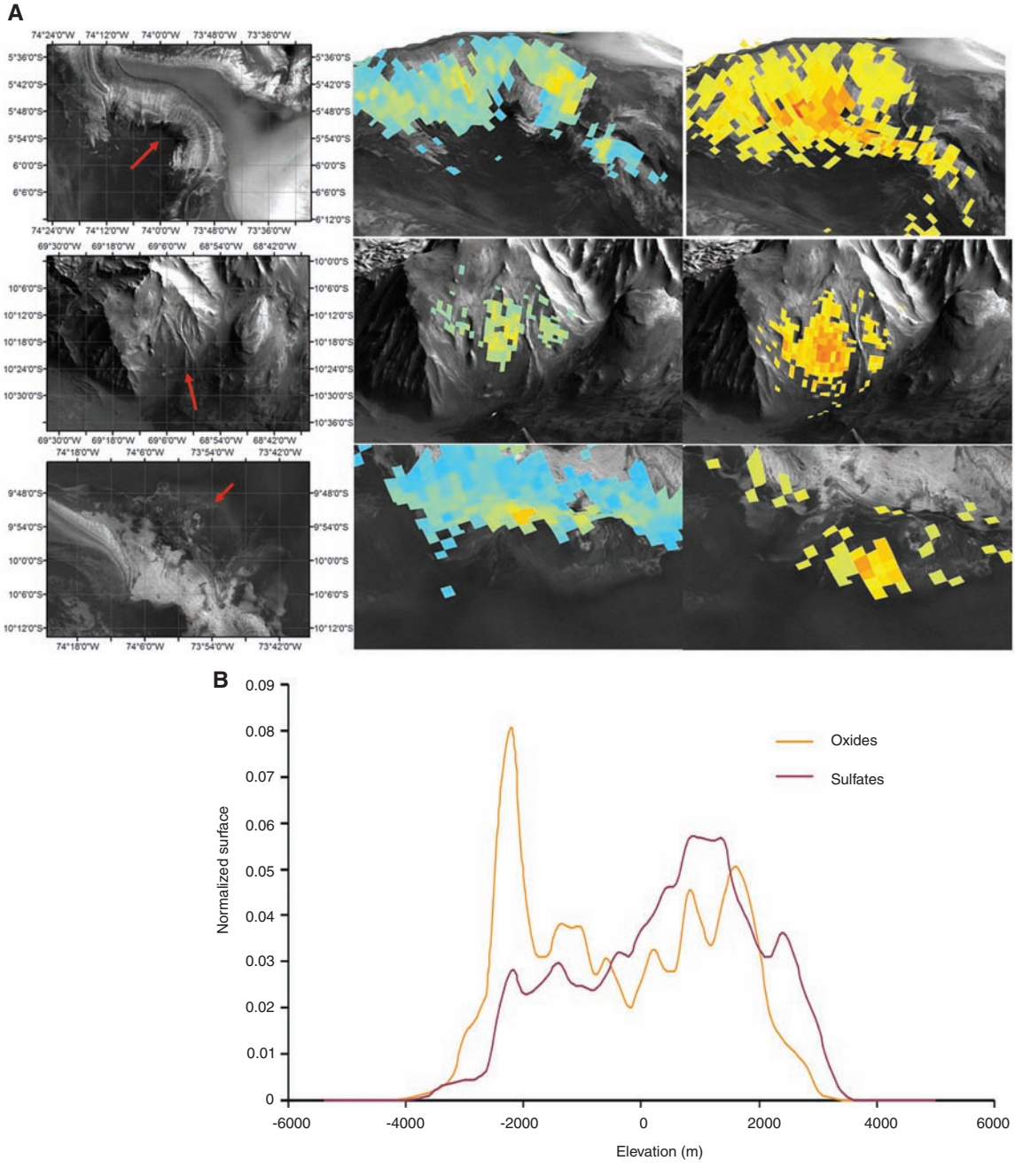

Fig. 3. Oxides and sulfates. (**A**) (Left) Geographic context with the arrow showing the direction of observation chosen for the three-dimensional (3D) views; the center positions are at 5°54′S, 74°W (top); 10°18′S, 69°W (middle); 10°S, 74°W (bottom). (Middle) Sulfate band depth (top: 2.1-μm band for kieserite; middle and bottom: 1.9-μm band for polyhydrated sulfates; blue = 3%, red = 10% and above). (Right) Oxide band depth (yellow = 10%, red ≥ 30%). The images are overlaid on a 3D view of High-Resolution Stereoscopic Camera images from orbits 360, 515, and 334 from top to bottom. (**B**) Distribution of oxides and sulfates versus altimetry in Melas Chasma. The distributions have been normalized by their area for comparison. For example, in the studied area, 8% of the ferric oxides are detected at elevations between −2200 and 2000 m. This diagram shows that oxides are located at similar and lower altimetry than the sulfates on a global scale.

the Etched Terrains and the hematite-bearing plains, whereas TES identifies hematite only in the hematite-bearing plains (*18*, *20*). In Valles Marineris, OMEGA identifications match TES identifications for some spots but not all (*20*). In Aram Chaos, the distribution of oxides as seen by OMEGA is very similar to the distribution of hematite identified by TES. Differences can occur because the visible and near-infrared wavelength range is most sensitive to red hematite, whereas the thermal infrared is most sensitive to coarse-grained hematite, which can be gray in color and not readily detectable at shorter wavelengths (*8*). It is also notable that a ferric absorption was identified in the Infrared Spectrometer for Mars/Phobos2 data (*21*), which matches the location of the westernmost deposit identified here in Candor Chasma.

Comparing ferric oxides with MGS/Mars Orbiter Laser Altimeter (*22*), MGS/Mars Orbiter Camera (*23*), and Odyssey/Thermal Emission Imaging System (*24*) images shows that the ferric oxides are associated with sulfate-rich interior layered deposits (ILDs) and extend to their base as low-albedo sand (Fig. 3). One layered deposit in Capri Chasma demonstrates this relationship particularly well (Fig. 4). Oxide-rich sand dunes are observed at the base of the ILDs. In Candor Chasma, oxide-rich sand is found as far as 2 km away from the base of the ILDs. This suggests that oxide-rich material is sand sized and is sufficiently resistant to survive long-distance transport. It seems that they are originally present in some ILDs and that erosion removal of soft sulfate concentrates ferric oxide.

Ferric oxides are identified by OMEGA over most of the martian surface (*3*); however, their spectral features differ substantially. The ferric oxides identified in the specific and distinct deposits discussed here show spectral signatures up to five times as deep as that of the anhydrous nanophase oxides constituting the bright dust, and they are spatially located and closely associated with sulfate deposits. We cannot entirely rule out that the differences merely reflect a much lower concentration of sulfates in the dust, to a level precluding the spectral features to be observed by OMEGA. Imaging at higher spatial resolution with the Compact Reconnaissance Imaging Spectrometer for MARS/Mars Reconnaissance Orbiter might validate this possibility. Our interpretation of OMEGA data favors a different formation mechanism for the ferric oxides observed in the dust and in the localized deposits described here.

Gas-solid interaction has been identified as a possible mechanism to form the nanophase oxides observed in martian bright regions (*3*). If gas-solid interaction was the principal process that produced these deposits, then one would expect that all light-toned deposits would be affected, which is not consistent with our observations. Alternatively, ferric oxides may have formed by fluid circulation at the surface or subsurface in many different environments (such as volcanic and sedimentary), either simultaneously with sulfates or as secondary phases (such as during later diagenetic alteration). They can exhibit a large variety of grain sizes, from nanophase particles in cement to large concretions

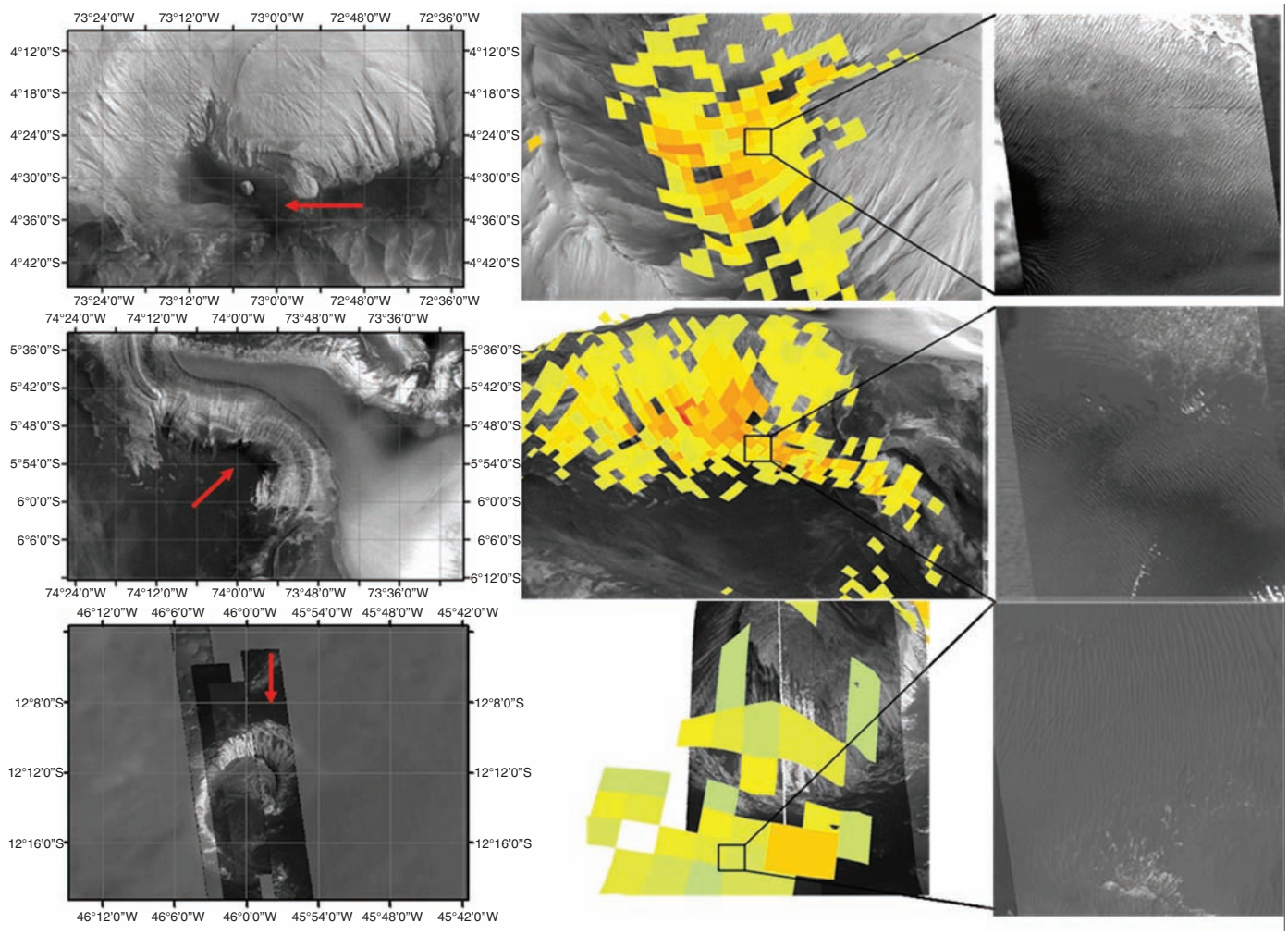

Fig. 4. Oxides are present on the ILDs and at their base, where we can observe oxide-rich sand dunes. (**Left**) Geographic location. The red arrow indicates the direction of observation used for the 3D views; the center positions are at 4°30′S, 73°W (top); 5°54′S, 74°W (middle); 12°12′S, 46°W (bottom). (**Middle**) Views in 3D of areas of interest in Ophir Chasma (top), Candor Chasma (middle), and Capri Chasma (bottom). The oxide band depth is shown on a scale of yellow (10%) to red (≥30%). (**Right**) MOC images showing that oxides are also located in sand-rich areas.

centimetric in size (*25*). Acidic environments have been suggested during sulfate formation in Meridiani Planum (*11*) and Valles Marineris (*3*). Oxide formation is observed together with sulfate precipitation in acidic environments (*26*, *27*). Hematite and sulfate formation are observed during hydrothermal alteration of basaltic tephra under acid-sulfate conditions on Mauna Kea volcano, Hawaii (*28*). Alternatively, diagenesis resulting from iron-rich fluid circulation can lead to large amounts of hematite cement or concretions (*25*). This has been interpreted in Terra Meridiani by the Opportunity Rover Team (*11*), where oxide formation occurs after sulfate formation (*29*, *30*). Sulfates are observed in Valles Marineris on outcrops several kilometers thick, much thicker than in Terra Meridiani, which could have favored sulfate transformation through diagenesis. The presence of concretions in Valles Marineris, although not necessary, would account for all the observations: oxide signature (*31*), resistant material, and accumulation in dark sand. The erosion of sulfate-rich outcrops would have led to the accumulation of oxide concretions at lower altitudes.

Identification of spatial relationships between iron oxides and layered sulfate deposits within Valles Marineris and Margaritifer Terra, which mirror that observed at Meridiani both from orbit and in situ, is a strong indication that these minerals formed in close association, through a process that operated within a specific region of Mars. This is consistent with their origin coupled to the tectonic events following the building of Tharsis, with transient supplies of water cementing sulfates and growing concretions (*3*).

References and Notes

1. R. E. Arvidson *et al.*, *J. Geophys. Res.* **111**, E12S08 (2006).
2. J.-P. Bibring *et al.*, *European Space Agency Spec. Publ.* **1240**, 37 (2004).
3. J.-P. Bibring *et al.*, *Science* **312**, 400 (2006).
4. R. V. Morris *et al.*, *J. Geophys. Res.* **105**, 1757 (2000).
5. D. M. Sherman, R. G. Burns, V. M. Burns, *J. Geophys. Res.* **87**, 10169 (1982).
6. R. V. Morris *et al.*, *J. Geophys. Res.* **90**, 3126 (1985).
7. R. V. Morris, H. V. Lauer, *J. Geophys. Res.* **95**, 5101 (1990).
8. M. D. Lane, R. V. Morris, S. A. Mertzman, P. R. Christensen, *J. Geophys. Res.* **107**, 5126 (2002).
9. R. V. Morris, D. C. Golden, J. F. Bell III, *J. Geophys. Res.* **102**, 9125 (1997).
10. R. V. Morris, D. C. Golden, *Icarus* **134**, 1 (1998).
11. S. W. Squyres *et al.*, *Science* **306**, 1698 (2004).
12. G. Klingelhöfer *et al.*, *Science* **306**, 1740 (2004).
13. J. K. Crowley *et al.*, *Geochem. Explor. Environ. Anal.* **3**, 219 (2003).
14. J. M. Sunshine, C. M. Pieters, *J. Geophys. Res.* **95**, 6955 (1990).
15. J. F. Mustard, J. M. Sunshine, *Science* **267**, 1623 (1995).
16. J. B. Adams *et al.*, *J. Geophys. Res.* **91**, 8098 (1986).
17. A. Gendrin *et al.*, *Science* **307**, 1587 (2005).
18. R. E. Arvidson *et al.*, *J. Geophys. Res.* **108**, 8073 (2003).
19. R. E. Arvidson *et al.*, *Science* **307**, 1591 (2005).
20. P. R. Christensen, R. V. Morris, M. D. Lane, J. L. Bandfield, M. C. Malin, *J. Geophys. Res.* **106**, 23873 (2001).
21. P. E. Geissler, R. B. Singer, G. Komatsu, S. Murchie, J. Mustard, *Icarus* **106**, 380 (1993).
22. D. Smith *et al.*, *NASA Planetary Data System*, MGS-M-MOLA-5-MEGDR-L3-V1.0 (2003).
23. M. C. Malin *et al.*, Malin Space Science Systems Mars Orbiter Camera Image Gallery (www.msss.com/moc_gallery/).
24. P. R. Christensen *et al.*, *Space Sci. Rev.* **110**, 85 (2004).
25. M. A. Chan, B. Beitler, W. T. Parry, J. Ormö, G. Komatsu, *Nature* **429**, 731 (2004).
26. D. K. Nordstrom, C. N. Alpers, in *Reviews in Economic Geologists*, G. S. Plumlee, M. J. Logdson, Eds. (Economic Geology Publishing Company, Littleton, CO, 1999), vol. 6A, pp. 133–160.
27. N. J. Tosca *et al.*, *Earth Planet. Sci. Lett.* **240**, 122 (2005).
28. R. V. Morris *et al.*, *Earth Planet. Sci. Lett.* **240**, 168 (2005).
29. J. P. Grotzinger *et al.*, *Earth Planet. Sci. Lett.* **240**, 11 (2005).
30. S. M. McLennan *et al.*, *Earth Planet. Sci. Lett.* **240**, 95 (2005).
31. The steep raise in reflectance discussed here is located in the 1.0- to 1.4-μm wavelength range, which is outside Panoramic Camera wavelength range.

Supporting Online Material

www.sciencemag.org/cgi/content/full/1144174/DC1
Figs. S1 and S2

24 April 2007; accepted 25 July 2007
Published online 2 August 2007;
10.1126/science.1144174
Include this information when citing this paper.

Replication Origin Recognition and Deformation by a Heterodimeric Archaeal Orc1 Complex

Erin L. Cunningham Dueber,[1,2] Jacob E. Corn,[2] Stephen D. Bell,[3] James M. Berger[2]*

The faithful duplication of genetic material depends on essential DNA replication initiation factors. Cellular initiators form higher-order assemblies on replication origins, using adenosine triphosphate (ATP) to locally remodel duplex DNA and facilitate proper loading of synthetic replisomal components. To better understand initiator function, we determined the 3.4 angstrom–resolution structure of an archaeal Cdc6/Orc1 heterodimer bound to origin DNA. The structure demonstrates that, in addition to conventional DNA binding elements, initiators use their AAA+ ATPase domains to recognize origin DNA. Together these interactions establish the polarity of initiator assembly on the origin and induce substantial distortions into origin DNA strands. Biochemical and comparative analyses indicate that AAA+/DNA contacts observed in the structure are dynamic and evolutionarily conserved, suggesting that the complex forms a core component of the basal initiation machinery.

The common modular architecture of replication initiators suggests that initiator function shares a degree of mechanistic conservation across the different domains of life (*1*–*3*). All cellular initiators contain both canonical DNA binding domains and discrete adenosine triphosphatase (ATPase) modules. The conventional DNA binding domains assist in localizing initiators to replication origins, whereas the ATPase elements appear to mediate the higher-order assembly of initiator subunits at the origin (*4*–*12*). The particular ATPase domains used by initiators fall within the broad superfamily of AAA+ proteins, which share an ability to form large multisubunit complexes that reconfigure the structural states of specific target macromolecules (*13*). Precisely how initiators use the AAA+ architecture to remodel origin structure remains unclear; however, initiator complexes have been shown to load replisomal factors onto DNA (*14*, *15*) and to facilitate origin unwinding in bacteria (*5*).

The archaeon *Sulfolobus solfataricus* uses three origins of replication (*oriC1*, *oriC2*, and *oriC3*) (*12*, *16*), with *oriC2* containing binding sites for all three of the organism's Cdc6/Orc1 initiator paralogs (Orc1-1, Orc1-2, and Orc1-3; Fig. 1A) (*17*). Previous studies suggest that Orc1-1 and Orc1-3 bind during the initiation of DNA replication and that Orc1-2 may act as a negative regulator (*12*). Although Orc1-1 recognizes an origin DNA repeat sequence known as the origin recognition box (ORB) (*11*, *12*), as well as a minimized version of this motif (mORB) found at *oriC2*, Orc1-2 and Orc1-3 each bind separate repeat sequences that are distinct from the mORB sites (termed C2 and C3, respectively). A 6–base pair (bp) overlap occurs between a mORB and a C3 site, creating a dual-site sequence jointly recognized by both Orc1-1 and Orc1-3 (Fig. 1A and fig. S1). To understand the molecular determinants by which initiators recognize and reshape origins, we cocrystallized Orc1-1 and Orc1-3 with a 33-bp DNA encompassing the mORB/C3 dual site (*18*). The structure was solved by multiwavelength anomalous dispersion (MAD) using

[1]Miller Institute for Basic Research in Science, 2536 Channing Way 5190, University of California, Berkeley, CA 94720, USA. [2]Department of Molecular and Cell Biology, QB3 Institute, Stanley Hall 3220, University of California, Berkeley, CA 94720, USA. [3]Medical Research Council (MRC) Cancer Cell Unit, Hutchison MRC Research Centre, Hills Road, Cambridge CB2 2XZ, UK.

*To whom correspondence should be addressed. E-mail: jmberger@berkeley.edu